ELSEVIER

Polymer 41 (2000) 7523–7530

polymer

Cavitation in strained polyvinylidene fluoride: mechanical and X-ray experimental studies

S. Castagnet[a,*], S. Girault[1,b], J.L. Gacougnolle[a], P. Dang[2,c]

[a]*LMPM-ENSMA, BP 109, 86960 Futuroscope Cedex, France*
[b]*CAL, Elf-Atochem, 95 rue Danton, 92300 Levallois Perret, France*
[c]*CERDATO, Elf-Atochem, 27470 Serquigny, France*

Received 29 October 1998; received in revised form 8 March 1999; accepted 21 January 2000

Abstract

PolyVinylidene Fluoride (PVDF) is a polar crystalline polymer commonly found in the apolar α crystalline form studied here. The complementarity of a macroscopic (tensile tests at constant crosshead speed) and a microscopic approach (Small-Angle X-ray Scattering and Wide-Angle X-ray Scattering) specifies the cavitation phenomenon occurring in this material when strained. At room temperature, micro-voids nucleate predominantly in equatorial intraspherulitic amorphous layers, just before the yield. For further strains, these defects grow in the tensile direction and damage affects a larger area of spherulites. This process, combined with classical amorphous shear mechanisms, prevails in PVDF deformation as crystallite fragmentation remains of minor importance, for axial strains of up to 30%.

Keywords: Polyvinylidene fluoride; Cavitation; X-ray

1. Introduction

For several decades, research projects dealing with PVDF were mostly interested in the piezoelectric properties of its β crystalline phase and, although apolar α PVDF is used in structural applications (off-shore, chemical industry, …), its mechanical behaviour was not studied extensively. Like in other crystalline polymers (PolyEthylene (PE), Poly(Propylene) (PP) [1], PolyOxyMethylene (POM) [2,3], …), a whitening affects this material when strained. This increased scattering is regarded by many authors [1,4–7] as the macroscopical evidence of cavitation and/or microcracking process. The aim of this paper is to highlight deformation micromechanisms in α PVDF (cavitation process, crystallites fragmentation,…) at room temperature.

Two complementary approaches are presented here: a macroscopic one based on mechanical tensile tests which confirm micro-voids existence in strained material, and a microscopic one based on wide and small angle X-ray scattering. Most mechanical approaches dealing with polymer damage (cavitation in toughened amorphous [8,9] or crystalline [10] polymers, copolymers [11], …) are based on volume change measurements [12] during uniaxial deformation. The technique applied in this study uses simultaneous measurements of the principal strains. The microscopic study is achieved by measuring the Small-Angle X-ray Scattering (SAXS) or the Wide-Angle X-ray Scattering (WAXS) patterns at selected points on the load–extension curve.

2. Material

The α PolyVinylidene Fluoride (PVDF) studied in this paper was provided by Elf-Atochem. The monomer involved in this thermoplastic is $-[CH_2-CF_2]-$. Its molecular weight distribution, determined by Gel Permeation Chromatography (GPC), is $M_w \approx 150\,000$ g/mol and $M_n \approx 80\,000$ g/mol meaning that a molecular chain (about 0.35 μm) consists of about 2350 monomers. This crystalline polymer exhibits a spherulitic structure characterized by SALS (Small Angle Light Scattering); the spherulite diameter is about 4 μm. Differential Scanning Calorimetry (DSC) (Fig. 1(a)) experiments indicate a crystallinity ratio of about 55%. As in many other crystalline polymers (PE, PP, …) two amorphous phases, called free amorphous (free chains and cilia) and constrained amorphous (tie molecules

* Corresponding author. Tel.: + 33-5-49498217; fax: + 33-5-49498238.
E-mail address: polymere@1mpm.ensma.fr (S. Castagnet).
[1] Tel.: + 33-1-47591359; fax: + 33-1-47591441.
[2] Tel.: + 33-2-32466882; fax: + 33-2-32466889.

0032-3861/00/$ - see front matter
PII: S0032-3861(00)00077-X

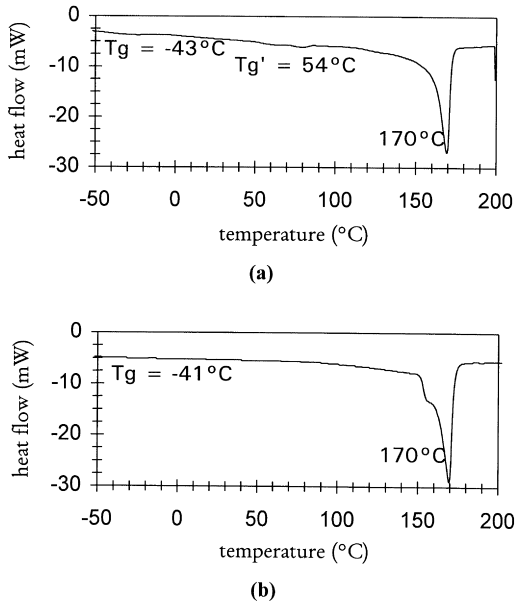

Fig. 1. DSC diagrams of PVDF: (a) as-produced; and (b) annealed at 150°C for an hour.

and folds), are distinguished in PVDF. Two relaxation processes can be observed both on Dynamical Modulus Analysis (DMA) (1.5 Hz) and DSC diagrams. The lower temperature process corresponds to the main glassy transition linked to the free amorphous phase: it occurs at $T_g = -43°C$. Concerning the higher temperature process (seen at $T' = 54°C$) it is unclear whether it can be attributed to the crystalline defect mobility or to the upper glassy transition linked to the constrained amorphous phase. This question is not discussed in this paper. It seems very difficult to us to make a strong distinction between these two mechanisms as an upper glassy transition implies a mobility process at the interface between amorphous and crystalline phases and probably requires some crystalline defect activation inside the crystal. In the present paper, the process occurring at T' will be seen as a higher mobility degree of chains no matter if they belong to the constrained amorphous phase or to local crystalline defects. The melting temperature is 170°C.

Samples used in X-ray experiments are annealed at 150°C for 1 h. It was ensured that no crystalline phase transition occurred during such a thermal treatment. After annealing, both the spherulite diameter and the crystallinity ratio remain constant. On the other hand, Fig. 1(b) clearly shows that the shape of the DSC curve is changed after annealing: the T' peak has disappeared and a shoulder on the endothermic melting peak has appeared at approximately 160°C. This modification shows the probable crystallization of the constrained amorphous phase in small crystals. In any case, the amorphous phase is supposed to be partially relaxed during this treatment which suppresses the thermomechanical history of the material.

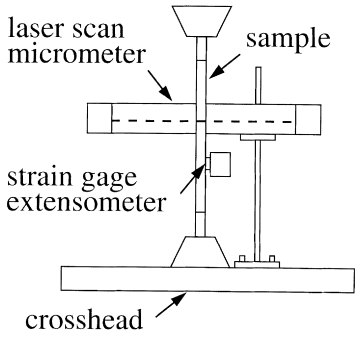

Fig. 2. Experimental device for volume strain measurements during tensile tests.

3. Experimental

3.1. Mechanical tests

Uniaxial tensile test are performed in this study. Dumbbell specimens are machined from PVDF 3 mm extruded sheets with specifications ISO R527 (gauge length 60 mm). All samples axes are oriented in the extrusion direction to avoid a possible texture effect. After machining, sections are polished and edges smoothed with several grades of fine emery paper. Tensile tests are carried out using an Instron Testing machine at constant crosshead speed.

A dilatometric method is developed to estimate the cavitation damage occuring in strained PVDF during tensile tests. It is based on the double extensometric system illustrated in Fig. 2. Axial and tranverse strains are measured using a classical strain gauge extensometer and a laser scan micrometer (wave length $\lambda = 670$ mm; resolution 0.1 μm), respectively. When needed, a chamber is added to regulate temperature to a constant value. It is pointed out that only two of the three principal strains ($\epsilon_{axial}, \epsilon_{width}, \epsilon_{thickness}$) are simultaneously available with this system. Isotropy of transverse strains ($\epsilon_{width} = \epsilon_{thickness}$) is experimentally proved: transverse strains measured along the thickness of a first set of samples are equal to transverse strains measured along the width of another set of samples strained under the same external conditions. Consequently, ϵ_{axial} and ϵ_{width} are sufficient for volume strain calculations, as indicated in Eq. (1):

$$\epsilon_{vol} = \epsilon_{axial} + \epsilon_{width} + \epsilon_{thickness} = \epsilon_{axial} + 2\epsilon_{width} \quad (1)$$

Two assumptions are made: (i) elastic process, shear bands and dilatational (cavitation) mechanisms linearly contribute to the total volume strain; and (ii) shear flow occurs at constant volume. Therefore, elastic and dilatational contributions to the overall volume strain can be separated according to Eqs. (2) and (3) knowing the mechanical constants of the material E (Young's modulus) and ν (Poisson's ratio).

$$(\epsilon_{vol})_{elastic} = (1 - 2\nu)\frac{\sigma_t}{E} \quad (2)$$

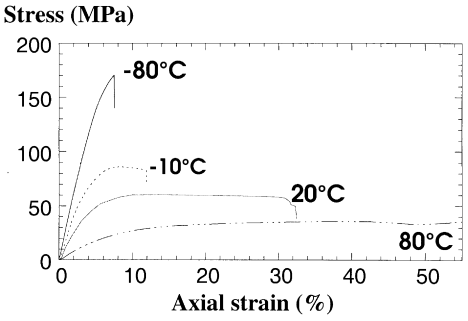

Fig. 3. $\sigma-\epsilon$ curves for tensile tests performed on PVDF over a wide range of temperatures (strain-rate: $2.5\times10^{-3}s^{-1}$).

$$(\epsilon_{vol})_{cavitation} = \epsilon_{vol} - (1-2\nu)\frac{\sigma_t}{E} \quad (3)$$

In these two last equations, σ_t accounts for the true stress. σ_t can be calculated from the applied force F, the instantaneous sample width and the transverse strain isotropy (see Eq. (4)). True axial and transverse strains are calculated using the Hill definition as indicated in Eqs. (5) and (6).

$$\sigma_t = \frac{F}{lh} = \frac{F}{l_0 h_0\left(1+\frac{\Delta l}{l_0}\right)^2} \quad (4)$$

$$\epsilon_{axial} = \ln\left(1+\frac{\Delta L}{L_0}\right) \quad (5)$$

$$\epsilon_{transverse} = \ln\left(1+\frac{\Delta l}{l_0}\right) \quad (6)$$

In Eqs. (4)–(6), L, l and h stand for instantaneous length, width and thickness, respectively. Index $_0$ refers to the initial values.

3.2. X-ray experiments

X-ray scattering experiments are performed in transmission mode by using a CuKα radiation (1.54 Å) from a rotating anode generator (RU-200, Rigaku Ltd) operated at 40 kV and 30 mA. SAXS and WAXS patterns are collected on image plates put at variable distances from the sample, typically 1.30 m for SAXS and 0.10 m for WAXS. Samples are drawn in situ in the X-ray set-up at selected points on the load–extension curve and are exposed to X-rays. The extension rate is 0.2 mm/min, and at each selected point, 1 h relaxation is performed before the X-ray exposure of 2 h. Deformation is held during the relaxation and the following exposure.

On SAXS patterns, the observed diffusion has two contributions:

- Amorphous and crystalline lamellae, which define the long spacing (L_p), lead to a peak observed at $q = 2\pi/L_p$. The integrated intensity of this peak depends on $(\rho_c-\rho_a)^2$, where ρ_c and ρ_a are the electronic density of crystalline and amorphous lamellae, respectively.
- Voids are responsible for an important contribution not necessary localized at a peak. Its intensity is very high because the contrast is linked to $(\rho_m-\rho_{voids})^2\rho_m$ is the mean electronic density of the polymer and ρ_{voids}, the electronic density of voids, is zero.

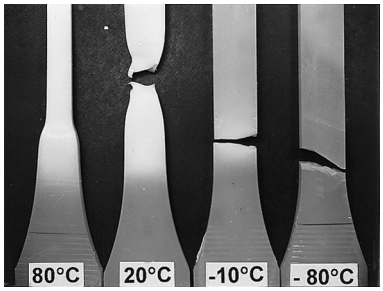

Fig. 4. Samples strained at different temperatures (strain-rate: $2.5\times10^{-3}s^{-1}$) (see Fig. 3 for $\sigma-\epsilon$ curves).

The Lorentz correction is applied to all the SAXS data presented in this paper. It means that the intensity is multiplied by q^2 where q is the scattering vector $q = (4\pi\sin\theta)/\lambda$. This correction, necessary for samples consisting of randomly oriented lamellae stacks [13], must therefore be applied for undeformed and weakly deformed samples. When the sample is highly deformed, lamellae stacks are supposed to be oriented perpendicularly to the tensile direction, and the Lorentz correction is questionable.

WAXS patterns show the evolution of the PVDF crystalline structure. Each peak corresponds to a reticular distance d_{hkl} of the structure. Initially, all crystallographic planes are randomly oriented, therefore the Bragg peaks are isotropic. After deformation, Bragg rings can turn into arcs, indicating an orientation of the crystallographic planes. The Bragg peak width can also change during deformation. Using the Scherrer formula [14] (7), it is linked to the crystalline size:

$$L_{hkl} = \frac{0.9\lambda}{\Delta 2\theta\cos\theta} \quad (7)$$

where: λ is the X-ray radiation wave length; $\Delta 2\theta$ the Bragg peak width at half maximum; 2θ the Bragg angle defined by $2d_{hkl}\sin\theta = \lambda$; L_{hkl} the size of the crystal in the direction perpendicular to d_{hkl}.

4. Results and discussion

4.1. Macroscopic approach

As in other crystalline polymers, whitening occurs in strained PVDF. This increased scattering is usually attributed to the nucleation and growth of micro-voids in the material. Our aim in this macroscopic mechanical approach is to clarify and quantify this phenomenon. To get a general idea of the mechanical behaviour of PVDF, several tensile tests

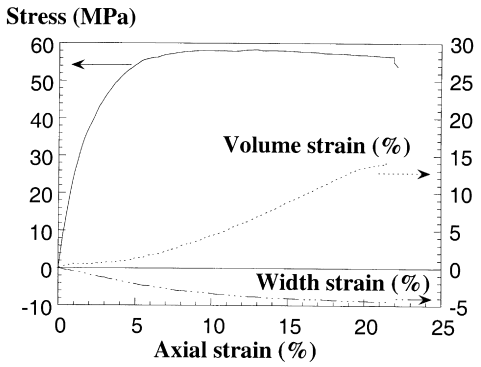

Fig. 5. Evolution of true stress, transverse and volume strains during tensile test ($T = 23$°C; strain-rate: 2.5×10^{-3}s^{-1}).

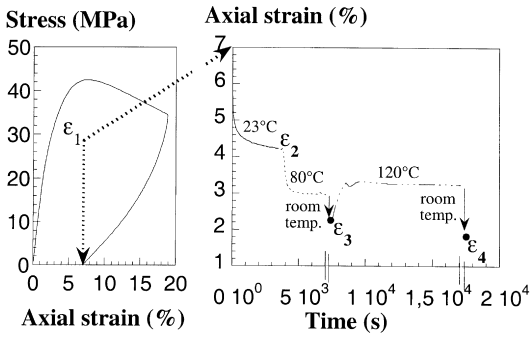

Fig. 6. Successive stages for measurement of the permanent axial strain of a PVDF sample strained at room temperature up to 19% (strain-rate: 1.5×10^{-3}s^{-1}).

are performed at 2.5×10^{-3} s^{-1}(on a wide temperature range including the two transition temperatures ($T_g = -43$°C; $T' = 58$°C). Results are presented in Fig. 3 and photographs corresponding to strained samples in Fig. 4. Three ranges of mechanical behaviour can be identified.

- $T < T_g$

Below the main glassy transition, the whole amorphous phase is glassy. The mechanical behaviour of PVDF is brittle. Fracture occurs with numerous fragments. No whitening is observed before fracture.

- $T_g < T < T'$

In this temperature range, the free amorphous phase is rubbery. The constrained amorphous and/or the first crystalline defects inside crystallites have no mobility. The mechanical behaviour becomes ductile. While PVDF deformation is still homogeneous, more or less stress whitening affects the sample. Then, for sufficiently high temperatures (typically 20°C here), necking can be observed. Fracture occurs in the neck immediately after deformation localization.

- $T' < T$

At these temperatures, the mobility of the whole amorphous phase and perhaps of some chains inside the crystal is increased. The mechanical behaviour is still ductile. Necking now propagates. Similar whitening appears during homogeneous deformation and persists in the neck propagation area.

These observations corroborate the statement that whitening involves amorphous phase relaxation. Molecular mobility increases with temperature. It can be concluded that a high enough degree of chain mobility is required to observe whitening. In particular, it is necessary for the free amorphous phase to be relaxed and for the constrained amorphous phase to acquire a certain degree of mobility as well. This is clear comparing tests carried out at −10°C and 20°C: whitening is much more pronounced in the latter case.

At this stage, the origin of whitening is not defined yet. If cavitation is responsible for this whitening phenomenon, it is expected, as a dilatant mechanism, to induce volume changes. This idea legitimates the calculation of volume strain from double extensometric strain measurements. We consider now a tensile test performed at 1.5×10^{-3}s^{-1} at room temperature. Evolutions of true stress (left vertical axis), transverse and volume strains (right vertical axis) are presented as a function of axial strain in Fig. 5. At the beginning ($\epsilon_{axial} < 1\%$), the behaviour is elastic; mechanical constants are estimated to be 2170 MPa for the Young's modulus and 0.36 for the Poisson's ratio. Since this last parameter is lower than 0.5, the volume strain increases but, at this stage, it is fully elastic. For axial strains from 1 to 5%, deformation in PVDF occurs at constant volume. For axial strains higher than 5%, the dilatational contribution to volume strain indicates that cavities nucleate in PVDF. This critical deformation value (lower than the yield strain determined for $\epsilon_{axial} = 7\%$), corresponds to the whitening apparition. For axial strains higher than 13%, the volume strain increase is more pronounced. The transverse strain evolution indicates that the cross sectional area is nearly constant: in this stage, PVDF deformation mainly occurs by extension of micro-voids in the tensile direction.

This experiment implies that whitening in strained PVDF is actually linked to the nucleation and growth of microcavities. Since the viscosity of the relaxed amorphous phase is lower than that of the crystalline phase, these defects are expected to form in the relaxed amorphous phase. However, our macroscopic approach gives no information about the exact location of these voids, their shape or their evolution. The following microscopic approach will answer these open questions.

In the previous paragraphs, we were not interested in the crystallite parts in PVDF deformation mechanisms. In this macroscopic approach, crystallite fragmentation, bound to occur when the polymer is strained, is studied through the permanent axial strain remaining even after annealing at temperatures higher than T'. Tensile and recovery tests illustrated in Fig. 6 are carried out. A PVDF sample (previously annealed at 120°C for 4 h) is loaded at room temperature at

Table 1
Permanent axial strain of PVDF samples strained at room temperature up to 11 and 19% (strain-rate: $1.5 \times 10^{-3} s^{-1}$) (see Fig. 4)

ϵ_{max} (%)	ϵ_1 (%)	ϵ_2 (%)	ϵ_3 (%)	ϵ_4 (%)
11	2.9	1.4	0.7	0.2
19	7	4.2	2.3	1.8

$1.5 \times 10^{-3}\ s^{-1}$ up to an axial strain ϵ_{max}. Then, it is unloaded at the same strain rate: the remaining axial strain of the sample is ϵ_1. At the end of the following recovery stage at room temperature, the remaining axial strain is ϵ_2. To accelerate the process, two recovery stages are performed first at 80°C and then at 120°C. At the end of each stage, the sample is brought back to room temperature to compare

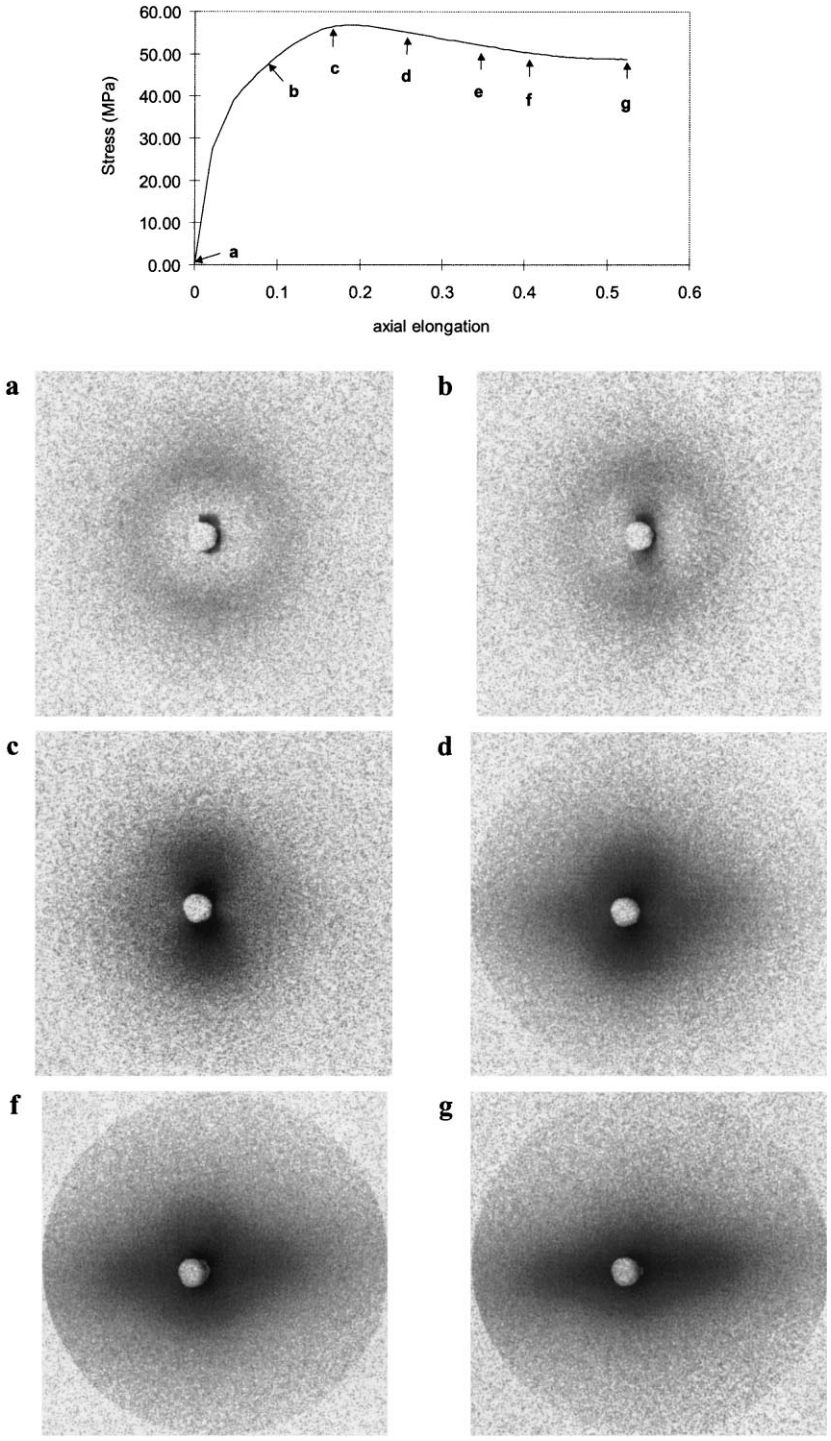

Fig. 7. Series of SAXS patterns, along the load–extension curve for PVDF films (800 μm thick). The points at which the X-ray scattering patterns were obtained are marked on the load–extension curve. The tensile axis is vertical.

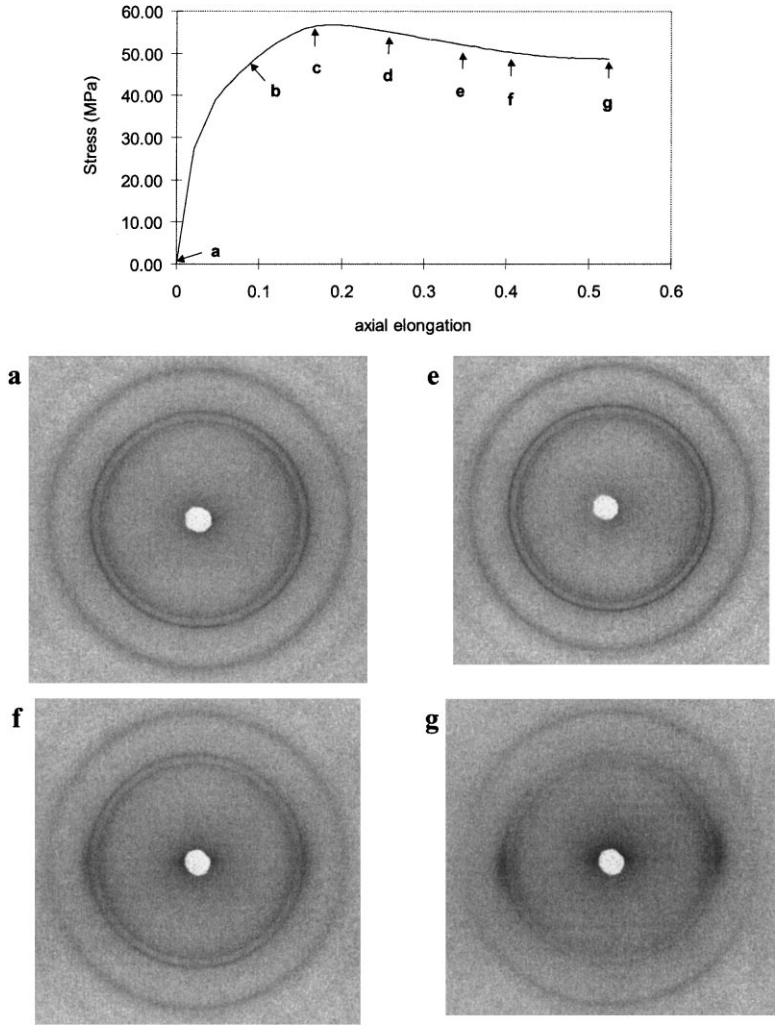

Fig. 8. Series of WAXS patterns, along the load–extension curve for PVDF films (800 μm thick). The points at which the X-ray scattering patterns were obtained are marked on the load–extension curve. The tensile axis is vertical.

the remaining axial strains (ϵ_3 and ϵ_4 after annealing at 80 and 120°C, respectively) to previous values. The second annealing temperature is not randomly chosen: it can be deduced from DSC experiments that the temperature level of 120°C is close to the highest temperature allowed to accelerate amorphous recovery without starting crystallites fusion. To prevent amorphous relaxation interfering with the crystalline phenomenon studied here, samples are annealed at 120°C for 4 h before testing. Results from two tests corresponding to ϵ_{max} values of 11 and 19% are presented in Table 1. From the very low values of permanent axial strains measured after recovery, it can be concluded that crystallites fragmentation is a minor micromechanism in PVDF deformation at least up to 20%. In this strain rate and temperature range, shear and cavitation are the predominant deformation processes. Again, our conclusion about the role of crystallites results from a global macroscopic approach. Questions, like a possible crystalline phase transition or lamellae orientation, cannot be answered considering these experiments. On these points, the WAXS technique gives complementary information.

4.2. Microscopic approach

Both WAXS and SAXS experiments performed on as-extruded and annealed (150°C for an hour) PVDF before loading show that its crystalline structure is orthorhombic. Peaks found are indexed as (010), (200) and (110) in the orthorhombic α phase, using $a = 9.64$ Å, $b = 5.00$ Å and $c = 4.64$ Å. These characteristics are close to the cell parameters usually published [15]. In the SAXS pattern, one peak is observed, attributed to the lamellae long spacing. This peak position leads to a periodicity of $L_p = (125 \pm 5)$ Å.

4.3. SAXS

Sequences of SAXS patterns recorded at selected points of the load–extension curve are shown in Fig. 7, where the tensile direction is vertical. On the unloaded sample and just

before the yield point, the ring of lamellar scattering is observed. At the selected point -b-, diffuse scattering parallel to the tensile direction emerges. This point corresponds to the beginning of the whitening. At the yield point (-c- in Fig. 7), the intensity of this diffuse scattering increases and seems to be localized at $q \neq 0$.This q value corresponds to a distance ≥ 600 Å. After the yield point, this scattering, essentially parallel to the tensile direction and attributed to the localization of voids, is more intense than lamellar scattering. After the -d- point on the load–extension curve (Fig. 7), the intensity of the vertical scattering decreases and further scattering appears perpendicular to the tensile direction. This new diffuse scattering increases in intensity up to fracture.

4.4. WAXS

A WAXS sequence, at the same points on the load–extension curve, was performed. It is represented in Fig. 8. Only significant slides are presented here for the WAXS evolution. WAXS patterns are quasi-isotropic and no significant changes are observed in the Bragg positions up to the point -f-. After this point (around an axial elongation of about 40%), several phenomena can be observed. An important orientation of crystalline lamellae appears perpendicular to the tensile direction. A notable broadening of the Bragg peaks occurs along the equator. This evolution corresponds to a decrease of the crystal size in the lamellae plane. Using the Scherrer formula, the crystal size is 150 Å for unloaded PVDF, and 50 Å for an axial elongation of 50%. Along the meridian, only a small decrease of this size can be observed (150 Å initially and 130 Å for an axial elongation of 50%). These evolutions show a fracture of crystalline lamellae and an orientation of the fragmented crystallites perpendicular to the tensile direction. This mechanism starts for an axial elongation of about 30%. The whitening and the important increase of the SAXS intensity begin for an elongation of 10%. The creation of voids cannot be associated with the crystalline lamellae fracture. Voids nucleate first in amorphous lamellae as previously deduced from mechanical experiments.

5. Discussion

All these mechanical and structural characterizations lead to our model for PVDF deformation. The initial annealed material is composed of spherulites of about 4 μm in diameter. These spherulites are made of amorphous and crystalline lamellae stacked with a period of 135 Å. The crystalline size in the lamella plane is about 150 Å.

Just before the yield, a dilatant mechanism can be observed from the macroscopic measurement of volume strains. The onset of whitening and the beginning of a vertical diffuse scattering occur at the same time. These facts can be interpreted as the nucleation of cavities in the equatorial amorphous regions of spherulites.

After the yield point, the number of cavities increases. They are mainly responsible for the softening mechanical behaviour observed in tension. Cavities are localized in the amorphous regions of the equatorial zone with a characteristic distance of about 600 Å. The existence of this distance is associated with stress relaxation around micro-voids which prevents the creation of additional cavities in the relaxed volume.

After an elongation of about 25%, voids are elongated in the tensile direction generating the equatorial streak. This is consistent with the macroscopic approach where the damage evolution is shown to be very anisotropic. The number of voids increases with elongation. The damaged zone is extended to the polar areas of the spherulites: the central diffusion becomes more and more isotropic.

Up to this elongation, crystalline characteristics (cell parameters, size of crystalline domains) remain unchanged. After an elongation of 34%, the crystalline lamellae are split up; the crystal size strongly decreases. Crystalline fragments are oriented perpendicular to the tensile direction. Microfibrils are created and the low-density areas between them are responsible for the equatorial streak intensity observed.

Such a physical model is very similar to the deformation mechanisms proposed by Butler et al. [16] for linear PE. In their case, the onset of cavitation corresponds both to the yield and to the martensitic transformation from an orthorhombic cell to a monoclinic one. This aspect constitutes a difference between PVDF and PE. In our α PVDF, no crystalline phase transformation is evident. The same whitening phenomenon was observed for PP. It was established that the spherulitic microstructure quickly turns into a disordered phase (usually called smectic phase [17]). Therefore, a comparison between PVDF and PP is quite difficult.

The micro-voids considered in this study are localized in the intraspherulitic amorphous layers. Using a SAXS approach like ours, only defects from about 100 to about 1000 Å can be detected. It is possible that other undetected cavity populations, with larger diameters (several thousands Å), which are nucleated in the interspherulitic amorphous phase, can contribute both to the high volume increase and the whitening of the strained material.

6. Conclusion

In this study, it was shown that two complementary approaches, a macroscopic one based on mechanical tensile tests with volume strain measurements and a microscopic one based on X-ray experiments, are necessary to precisely describe the deformation and damage micromechanisms of α PVDF homopolymer at room temperature. The whitening phenomenon observed during elongation can be attributed to the nucleation and growth of micro-voids in the amorphous phase. These defects are created in the equatorial zones of spherulites before the yield point is reached. Their growth and the nucleation of cavities in other areas

of the spherulites are responsible for softening mechanical behaviour. The crystalline phase of the polymer remains unchanged for elongations up to about 40%. For higher elongations, crystalline lamellae are split up and oriented perpendicular to the tensile direction. Microfibrils are formed with very extended voids between them. No crystalline phase transition was observed.

Acknowledgements

The authors would like to gratefully acknowledge Mrs A. Ibos and Mr. P. Decourval, Centre d'Applications de Levallois, ELF-ATOCHEM, for their help in performing the X-ray experiments presented in this paper.

References

[1] Cessna LC. Polym Engng Sci 1974;14:696.
[2] Narisawa I, Ishikawa M. In: Kausch HH, editor. Crazing in polymers, Advances in polymer sciences, 91/92. Berlin: Springer, 1990. p. 353.
[3] Plummer CJC, Kausch HH. J Macromol Sci Phys B 1996;35:637.
[4] Friedrich K. In: Kausch HH, editor. Crazing in polymers, Advances in polymers science, 52/53. Berlin: Springer, 1983. p. 353.
[5] Volynskii AL, et al. Polym Sci 1991;33:917.
[6] Dettenmaier M, Kausch HH. Polym Bull 1980;3:571.
[7] Dettenmaier M, Kausch HH. Colloid Polym Sci 1981;259:937.
[8] Bucknall CB, Partridge IK, Ward MV. J Mater Sci 1984;19:2064.
[9] Dekkers MEJ, Heikens D. J Mater Sci 1985;20:3873.
[10] Bucknall CB, Heather PS, Lazzeri A. J Mater Sci 1989;16:2255.
[11] Hobbs SY, Dekkers MEJ. J Mater Sci 1989;24:1316.
[12] Naqui SI, Robinson IM. J Mater Sci 1993;28:1421.
[13] Baltà-Calleja FJ, Vonk CG. X-ray scattering of synthetic polymers. Amsterdam: Elsevier, 1989.
[14] Guinier A. Théorie et technique de la radiocristallographie. Paris: Dunod, 1956.
[15] Lando JB, Olf HG, Peterlin AJ. J Polym Sci A-1 1966;4:941.
[16] Butler MF, Donald AM, Ryan AJ. Polymer 1998;39:39.
[17] Kammer HW, Kummerloewe C, Greco R, Mancarella C, Martuscelli E. Polymer 1988;29:963.